Supplemental Information: *Interfacial Energy as an Approach to Designing Amphipathic Surfaces During Photopolymerization Curing*
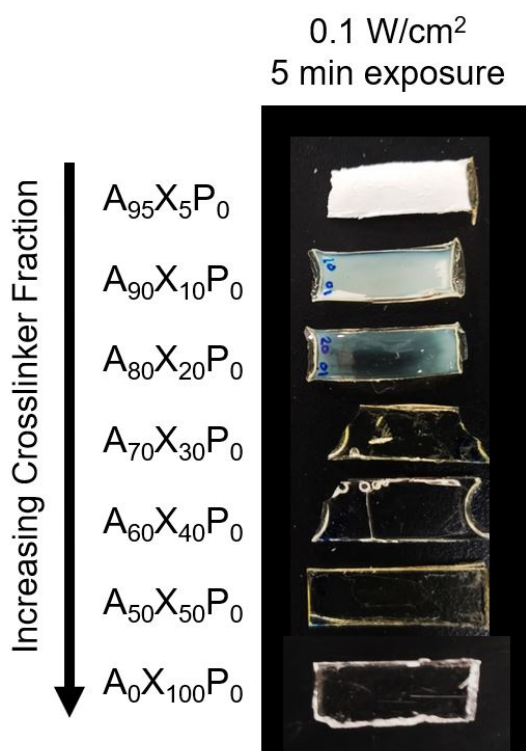

Figure S1: The HDDA crosslinker fraction was varied between 5 wt% to 100 wt% ($A_{95}X_5P_0$ to $A_0X_{100}P_0$) with respect to the acrylonitrile to identify a suitable comonomer system for studying PIPS. These comonomer resins were cured at 0.1 W/cm^2 for 5 minutes and subsequently annealed at 150° for 1 hour to maximize the extent of conversion. Opacity was observed in several of these samples, with the opacity most significant in samples with low HDDA fraction (e.g. $A_{95}X_5P_0$) and gradually decreases with increasing HDDA fraction. At a loading level of 30% HDDA ($A_{70}X_{30}P_0$), samples remain transparent throughout the copolymerization and annealing. The presence of opacity at the lower HDDA fractions indicates phase separation at a domain size larger than the wavelength of the interacting visible light [2, 41]. It is for this reason $A_{70}X_{30}P_0$ was chosen as the base resin in the study.
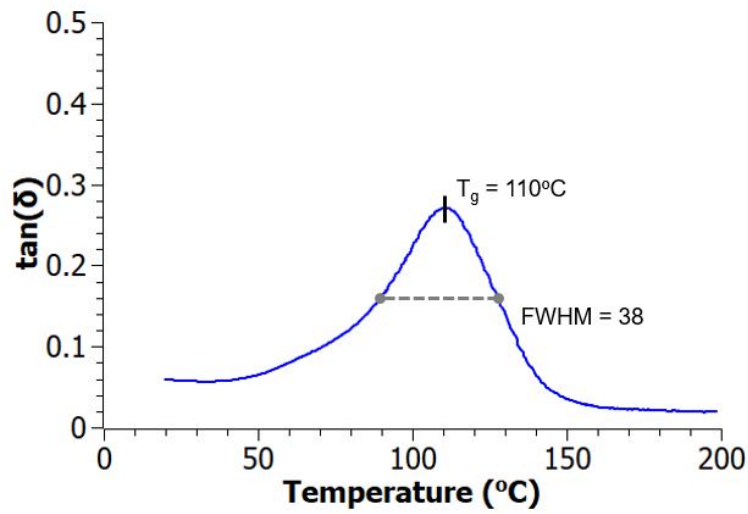
Figure S2: Tan(δ) profile for the $A_{70}X_{30}P_0$ baseline comonomer system. The glass transition (T_g) is 110°C with a full width half maximun (FWHM) of 38 degrees. The symmetric nature of the plot indicates a well mixed polymer network. The large FWHM indicates slight heterogeneity at the local network level, as has been discussed for free radical crosslinked systems and supported by the SAXS data in **Fig. S3a.**
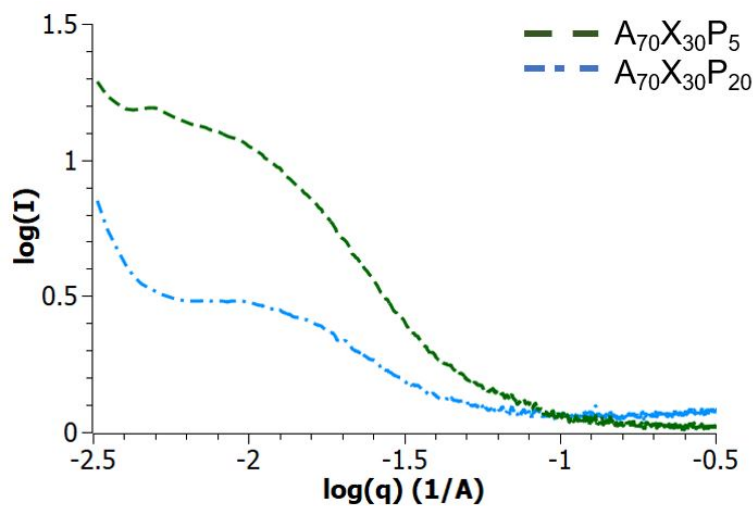

Figure S3: SAXS profiles for $A_{70}X_{30}P_c$ samples cured at 0.1 W/cm^2 confirm nanoscale heterogeneity within the investigated formulations. The domain size associated with nanoscale heterogeneity ranges between 70 nm and 100 nm for the PMMA loading fractions.
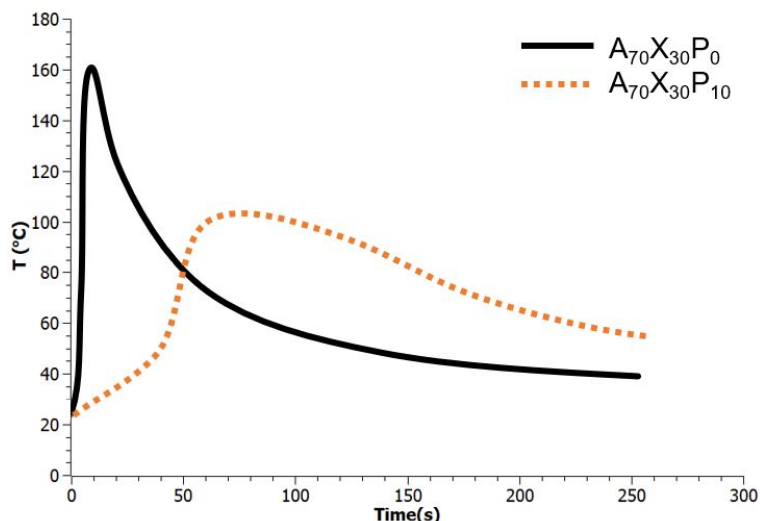
Figure S4: A thermocouple was used to log the temperature variation during polymerization of the control comonomer matrix $A_{70}X_{30}P_0$ as well as the medium PMMA loading condition $A_{70}X_{30}P_{10}$, utilizing the same rectangular sample geometry. Two main observations are clear from this analysis. First $A_{70}X_{30}P_0$ has a much higher exotherm (T_{max} of 160°C vs 103°C). Secondly, the time at which T_{max} occurs is much earlier $A_{70}X_{30}P_0$ compared to the PIPS resin $A_{70}X_{30}P_{10}$ (9 seconds vs 60 seconds). Additionally, the control resin exhibits a rapid release of energy from the heat of polymerization that then quickly decays. In contrast, heat from the reaction in the PIPS system is sustained for longer, keeping the sample environment hot. These observations point to a decrease in the evolved exotherm with PMMA loading, which is expected given the reduction in reactive double bonds within the resin as PMMA loading increases. While the polymerization heat impacts the diffusivity and mobility of species within the resin, the stark phase segregation observed in $A_{70}X_{30}P_{10}$ resins is not merely a result of a differing thermal environment. If the thermal environment (e.g. relative magnitude of T_{max}) determined phase structure, we would anticipate lower loadings of PMMA to yield more distinct phase domains as the higher T_{max} would facilitate diffusion. Given that the opposite is observed (e.g. more distinct phase domains at higher PMMA loadings), we can conclude that polymerization heat is not a determining factor.
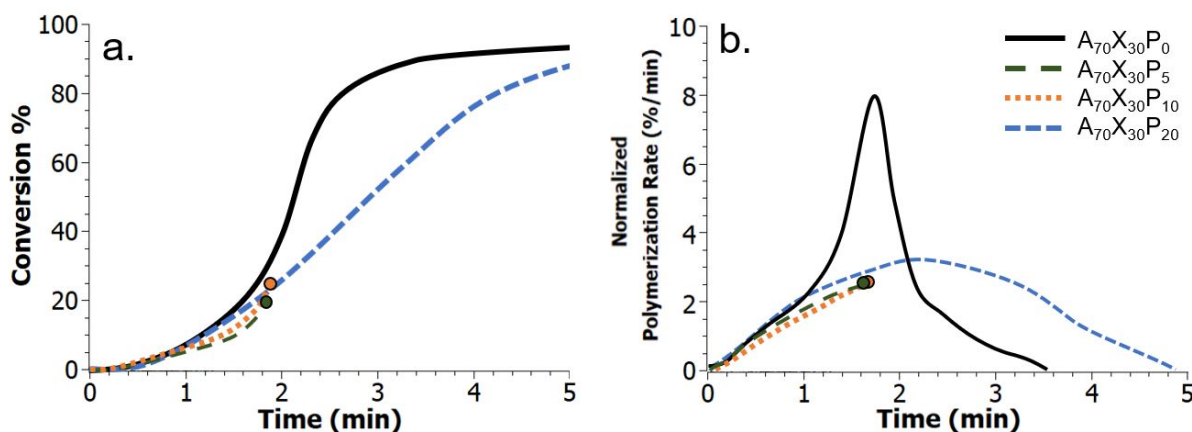

Figure S5: The conversion of monomer into polymer in $A_{70}X_{30}P_c$ is tracked by monitoring the disappearance of the C=C bond peak at 6165 cm^{-1} during the 0.1 W/cm^2 UV cure. A sharp S-shaped curve is observed in the Conversion % vs. time plot for $A_{70}X_{30}P_0$, consistent with autoacceleration behavior characteristic of the acrylate crosslinker used (a). IR signal detection stops at approximately 2 minutes for $A_{70}X_{30}P_5$ and $A_{70}X_{30}P_{10}$, indicating domains capable of scattering 1620 nm light have formed. The rate of polymerization is obtained by taking the derivative of the Conversion % plot with respect to time (b). The maximum polymerization rate is observed approximately halfway through the total reaction.

Table S1: Extent of Polymerization Using Toluene Removal of Unreacted Monomer

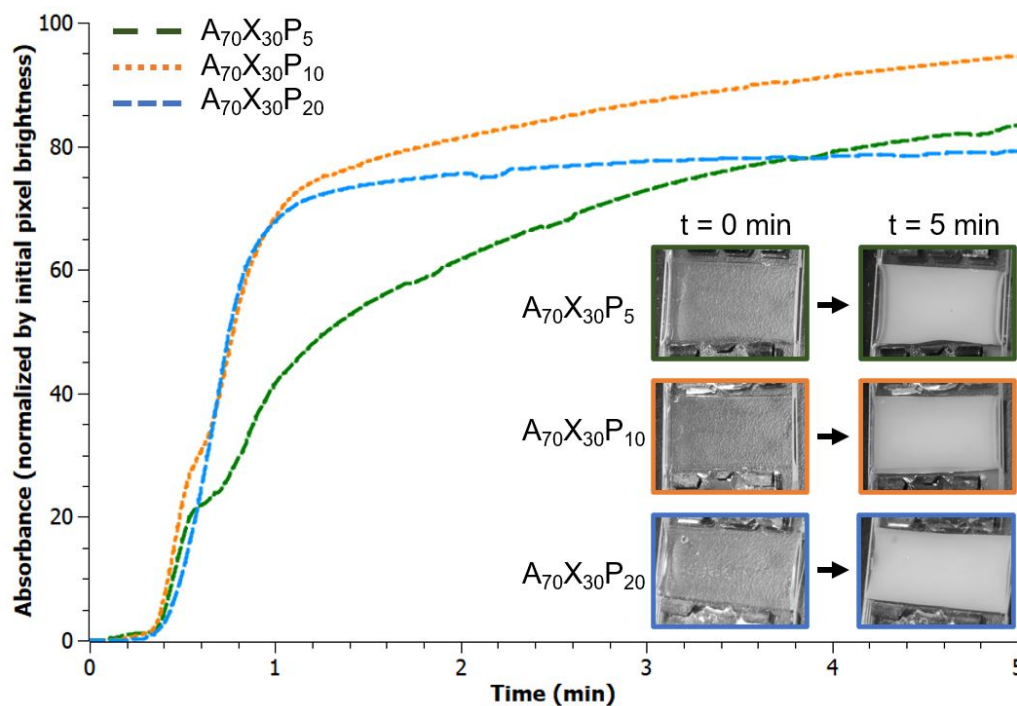|	Original Mass (g)	Mass After Solvent (g)	Difference in Mass (g)	Loss of Original Mass	Converted Monomer
$A_{70}X_{30}P_0$	0.0188	0.0176	0.0012	6.4 %	93.6 %
$A_{70}X_{30}P_5$	0.0158	0.0119	0.0039	24.7 %	75.3 %
$A_{70}X_{30}P_{10}$	0.0122	0.0087	0.0035	28.7 %	71.3 %
$A_{70}X_{30}P_{20}$	0.0341	0.0293	0.0048	14.1 %	85.9 %

Figure S6: Tracking sample opacity onset with time over the photopolymerization was recorded by optical observation. A greyscale video (30 frames per second) was taken for each sample against a black background throughout the curing process. The change in opacity was calculated using ImageJ to make a rectangle around the sample area and average the pixel brightness for each frame of the video, allowing us to plot the increase in average pixel brightness with time. Because each resin is fully transparent before curing, the average pixel brightness at the beginning is taken to have no absorbance. For the PIPS resins, onset of opacity is very rapid, occurring approximately 20 seconds after UV irradiation initialization.

Table S2: Miscibility Prediction Parameters

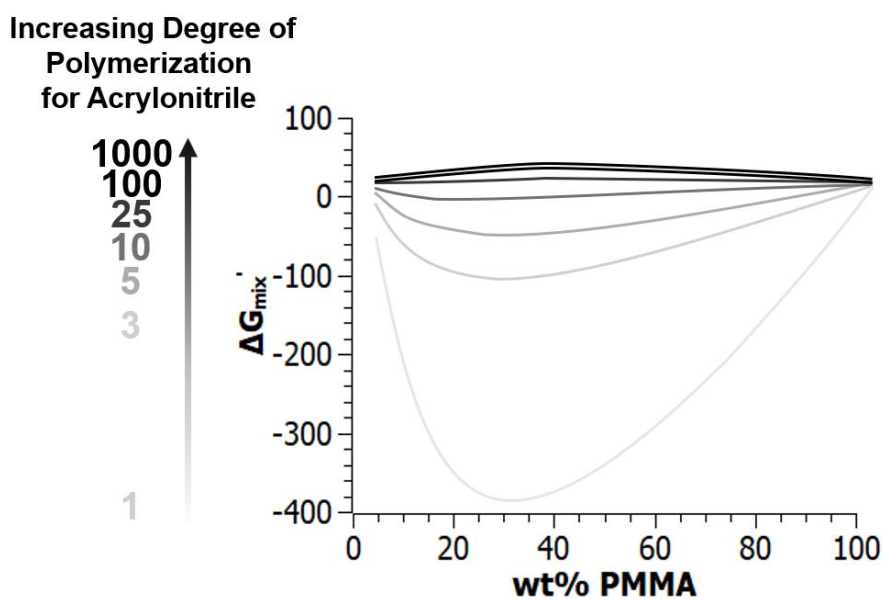|	Density (g/mL)	Solubility Parameter $(J^{0.5}/cm^{1.5})$	Degree of Polymerization (Repeat Units)	Repeat Unit MW (g/mol)	End Group MW (g/mol)
Acrylonitrile (AN)	0.81	21.4	1	53.06	0
Poly(methyl methacrylate) (PMMA)	1.18	23.1	1200	100.13	30.08

Figure S7: Calculations of the derivative of ΔG_{mix} can be done for oligomers of the reacting acrylonitrile as the reactive molecule increases its degree of polymerization. As the molecules grow, their solubility parameter can be estimated from the energy of cohesion associated with the functional groups present [50]. This enables us to identify at what point along the monomer to polymer transition does the PMMA additive favor phase separation based on the increase in $\Delta G'_{mix}$. More details about this approach can be found in references [47] and [48].
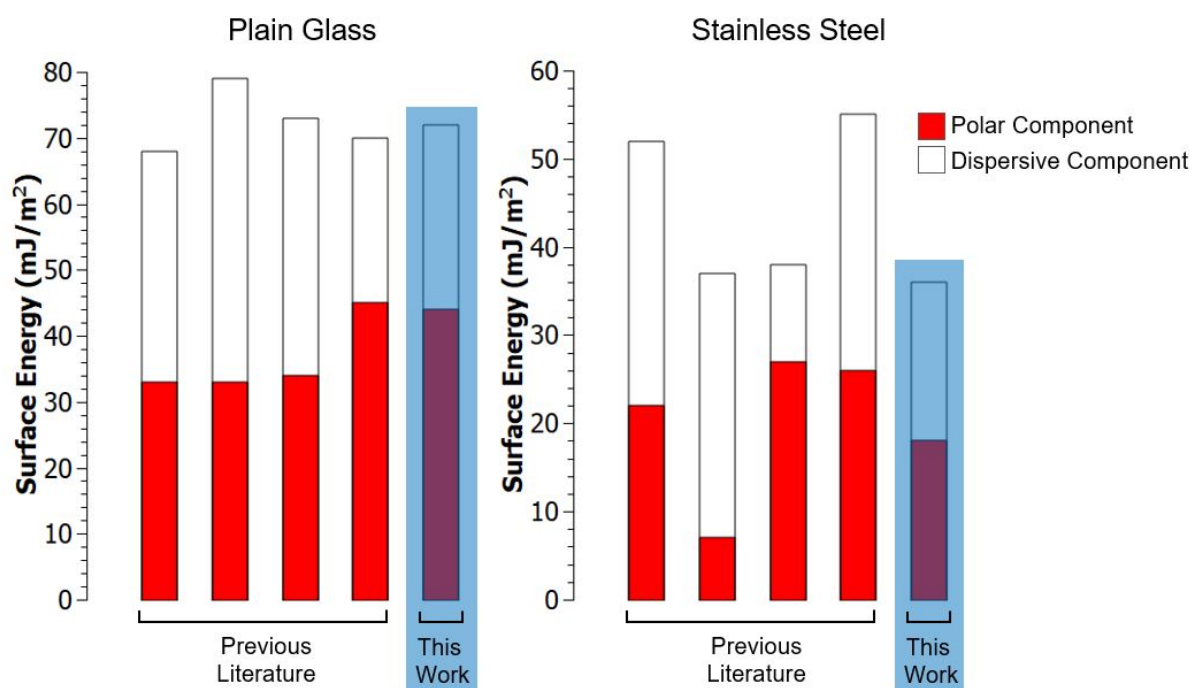
Figure S8: Each bar graph value represents measurements taken of respective substrates by various researchers using a goniometer. The results of compiling these measurements highlight subjectivity in the range of possible total surface energy values along with the ratio of polar to dispersive components. Given that the surface energy values measured in this work for plain glass and stainless steel substrates fall within the range of previously reported literature, these values can be taken in confidence for the purpose of this study. Surface energy data for the glass was extracted from [53, 54, 55] and that for the stainless steel from [56, 57, 58].
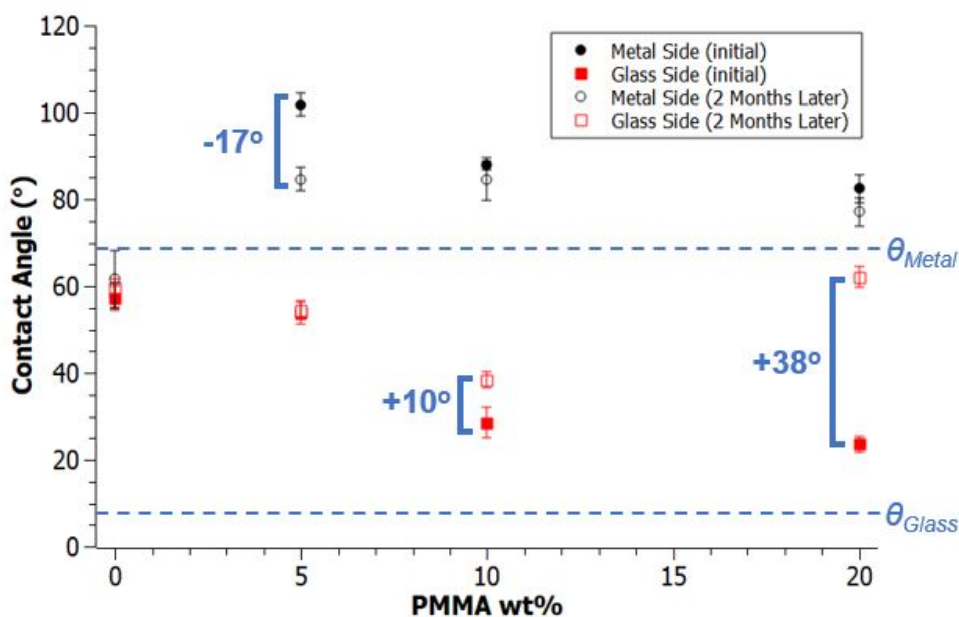
Figure S9: The long term stability of the metal/glass sample surfaces was checked by comparing contact angle measurements taken from the same samples immediately after photopolymerization and also after 2 months of storage. No statistical change is noted for the control samples containing zero PMMA polymer, however, samples containing PMMA polymer that resulted in macroscale phase separation exhibited significant changes in measured contact angle over the 2 month period. The increase in contact angle for $A_{70}X_{30}P_{10}$ and $A_{70}X_{30}P_{20}$ on the glass side interface can most likely be attributed to the increased mobility of PMMA chains at that surface, given they are not as rigidly (covalently) connected within the crosslinked network. This argument is strengthened by the jump from a 10° increase to a 38° increase in contact angle between $A_{70}X_{30}P_{10}$ and $A_{70}X_{30}P_{20}$, where there is a greater concntration of PMMA polymer present in the sample. The presence of the crosslinked network stabilizes the substrate-influenced sample surface character for a longer period than the plain polymer melts studies by Cuthrell, a change in surface character on the scale of months compared to hours [44].